Topical Editor Decision: Publish subject to revisions (further review by editor and referees) (30 May 2019) by Andrew J. Kavanagh

Comments to the Author:

Reviewer 1 is broadly happy with your responses and why you do not identify the 2nd troposphere. However they insist that you complete the four key points that they have identified prior to publication.

Reviewer 2 is less satisfied with your responses. The main sticking point appears to be your lack of discussion of a 2nd troposphere using middle mode. I think it is essential that you include a clear discussion of this in the paper including why the measurement is not possible for the radar. Reviewer 1 has accepted this, but I think reviewer 2 is concerned that the general reading audience might not appreciate the problem.

Once you have made the required changes I will reassess the manuscript and determine whether the reviewers really need to see it again (I would hope not if you do everything they now ask).

Dear Editor Kavanagh,

We thank you and both reviewers for the constructive comments, which as outlined have helped improve the manuscript. I totally agree with your points. Especially, according to the comments of reviewer 1 and reviewer 2, it is really necessary to explain clearly in the revised manuscript that the Beijing MST radar cannot detect tropopauses with altitudes above 16km, whether or not these are the first or second tropopause.

In addition, in order to make the 'cyan asterisks' in Figure 3 visible, the asterisks have been plotted in white in revised manuscript. The modified Figure 3 is given below.

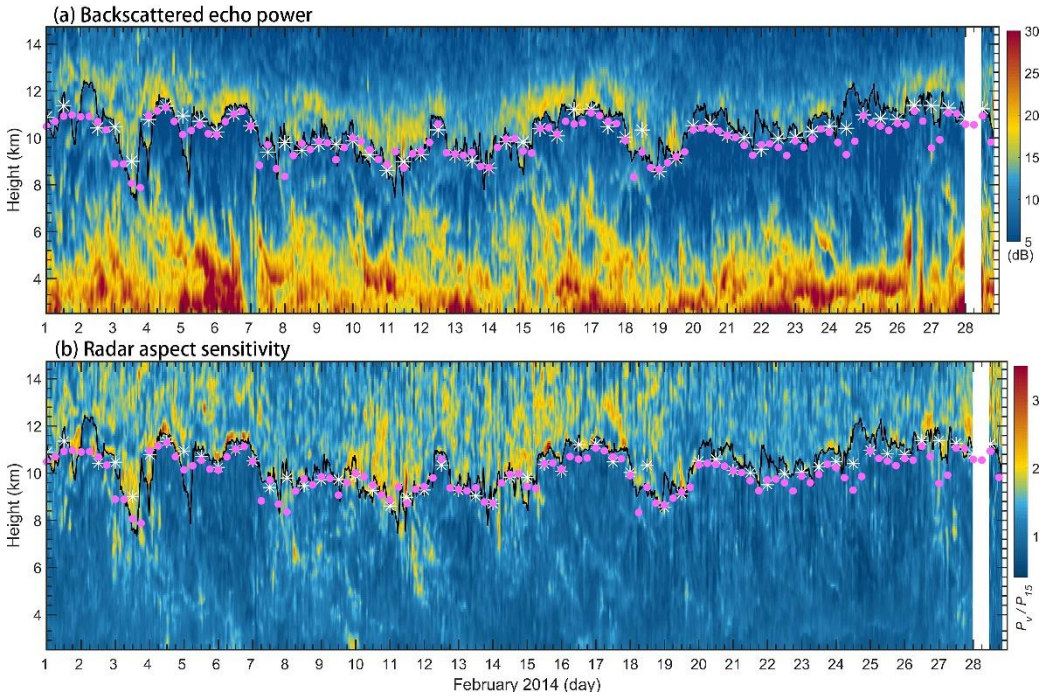

Detailed responses to the reviewers are given as follows. The revised manuscript with tracked changes is also attached later.

Response to reviewer #1

Second review of 'High-resolution Beijing MST radar detection of tropopause structure and variability over Xianghe (39.75° N, 116.96° E), China', by Chen et al.

Note that in my comments below, I refer to the manuscript which the authors have incorporate both Reviewers' comments from the first review round.

I thank the authors for considering and addressing my comments. It is now clear why Chen et al. have had to reject consideration of tropopauses with altitudes above 16km, whether or not these are the first or second tropopause. This is a pity, but clearly a limitation of the radar system's power and capabilities.

As such, once the authors have implemented the following minor points, I would find this manuscript acceptable for publication.

Dear Reviewer,

We really thank the reviewer for the second encouraging view of our work.

1) In your abstract, you need to clearly state that you only consider the lower tropopause altitudes. This is not mentioned at all at present but is a very important point to include in the abstract. I suggest words on line 19 such as: "We only consider tropopause altitudes below 16km in this study because of limitations with the radar system", or words to this effect.

Response:

Complied with, we agree that this is necessary to be mentioned in the abstract. Words " We only consider tropopauses below 16km in this study because of limitations with the radar system" has added in the abstract.

2) Line 214 describing Figure 5, I think a better way to say this is: 'Higher probabilities of large tropopause sharpness values occur when the RT-LRT difference is less than 0.5km"

Response:

Complied with the suggestion. The corresponding sentence describing Figure 5 has been changed to 'What is apparent is that higher probabilities of large tropopause sharpness values occur when the RT-LRT difference is less than 0.5km'.

3) Line 248: I can't see from Figure 7 that the 'radar power points' show less dispers[ion]. Please remove the words 'and radar power points'

Response:

Thanks for pointing this out. Complied with your suggestion and we have removed the words 'and radar power points' in the revised manuscript.

4) Figure 3. The 'cyan asterisks' which indicate the LRT location are practically invisible because

you are plotting a light blue color on to a dark blue color. I suggest you plot these asterisks in white, gold, or bright red. That should make them visible.

Response:

Thanks for your suggestion. The asterisks have been plotted in white in the revised manuscript.

Response to reviewer #2

I appreciate the effort of authors in revising the manuscript and providing good responses.

However, I am not totally satisfied with the revised version. Main concern is on the identification of second tropopause. This should be addressed by middle mode radar observations. Reviewer#1 also suggested to examine both the thermal tropopause (first and second LRT) using low mode and middle mode MST radar observations.

Though the focus of the study is on first troposphere, the authors should attempt to analyze the middle mode radar observations to identify the second tropopause, if exist. This should be added and discussed in the manuscript. Adding this would be a significant contribution to science/literature.

Dear Reviewer,

We really thank you for your helpful and constructive comments. If the second tropopause is present and sharpness enough, it should indeed be tried to detect the second tropopause using middle mode data. However, because of the limitations of the radar system itself (transmitted power, height resolution, etc.), second tropopauses with altitudes near 16 km or higher are not considered in this study.

In our first responses, we have given one month observation result (the month is same as that of Figure 3), which repeated here.

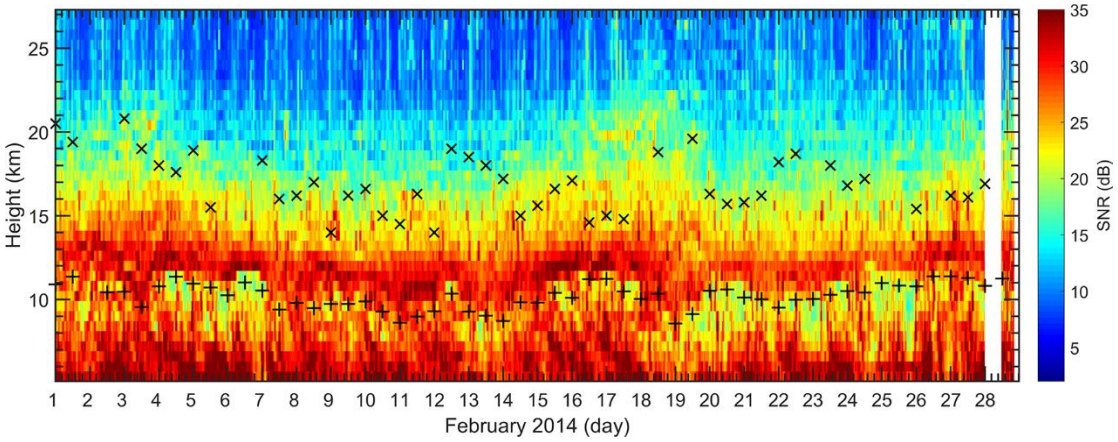

Figure R1. Middle mode observation results: Altitude-time intensity plot of radar backscattered echo power for February 2014. '+' indicates the first tropopause; and 'x' denotes the higher second tropopause derived from radiosonde data.

The results show that the first tropopause structure can be seen with middle mode

observations, but the boundary is unsharpness and too coarse to identify the clear tropopause height, at least (especially) compared to the Figure 3 in the manuscript. In addition, also is the most important feature, the second tropopause is barely detected by middle mode results.

In order to explain clearly in the revised manuscript that the Beijing MST radar cannot detect tropopauses (whether or not these are the first or second tropopause.) with altitudes above 16km, words "We only consider tropopauses below 16km in this study because of limitations with the radar system" and " In the present study, we focus only on the first tropopauses below 16 km and these will be referred to as ‘tropopause’ hereafter" have been added in the abstract and introduction respectively.

High-resolution Beijing MST radar detection of tropopause structure and variability over Xianghe (39.75° N, 116.96° E), China

Feilong Chen[1], Gang Chen[1*], Yufang Tian[2], Shaodong Zhang[1], Kaiming Huang[1], Chen Wu[1], Weifan Zhang[1]

[1]School of Electronic Information, Wuhan University, Wuhan 430072, China.

[2]Key Laboratory of Middle Atmosphere and Global Environment Observation, Institute of Atmospheric Physics, Chinese Academy of Sciences, Beijing 100029, China.

*Corresponding author: Gang Chen (g.chen@whu.edu.cn)

Abstract.

As a result of partial specular reflection from the atmospheric stable layer, the radar tropopause (RT) can simply and directly be detected by VHF radars with vertical incidence. Here, the Beijing MST radar measurements are used to investigate the structure and the variabilities of the tropopause in Xianghe, China with a temporal resolution of 0.5 hour from November 2011 to May 2017. High-resolution radar-derived tropopause is compared with the thermal lapse-rate tropopause (LRT) that defined by the World Meteorological Organization (WMO) criterion from twice daily radiosonde soundings and with the dynamical potential vorticity tropopause (PVT) that defined as the height of 2 PVU surface. We only consider tropopauses below 16km in this study because of limitations with the radar system. During all the seasons, the RT and the LRT in altitude agree well with each other with a correlation coefficient of ≥0.74. Statistically, weaker (higher) tropopause sharpness seems to contribute to larger (smaller) difference between the RT and the LRT in altitude. The RT agrees well with

the PVT in altitude during winter and spring with a correlation coefficient of ≥0.72, while the correlation coefficient in summer is only 0.33. As expected, the monthly mean RT and LRT height both show seasonal variations. Lomb-Scargle periodograms show that the tropopause exhibits obvious diurnal variation throughout the seasons, whereas the semidiurnal oscillations are rare and occasionally observed during summer and later spring. Our study shows the potential of the Beijing MST radar to determine the tropopause height, as well as present its diurnal oscillations.

Key words: VHF radar; MST radar; tropopause; diurnal oscillation.

1. Introduction

The tropopause marks a transition zone separating the well-mixed convectively active troposphere from the stably stratified and more quiescent stratosphere. Its structure and variability is characterized by large changes in thermal (e.g., lapse rate), dynamical (e.g., potential vorticity), and chemical properties (e.g., ozone and water vapor) and hence acts as a key role for the stratosphere-troposphere exchange (STE) processes (Hoinka, 1998; Seidel et l., 2001). The height of the tropopause depends significantly on the latitude, with about 17 km near the equator and less than 9-10 km at polar latitudes (Ramakrishnan, 1933). Over subtropical latitudes with the presence of subtropical jet, where the tropopause experiences rapid change or breaking, tropopause folding events are commonly observed (Pan et al., 2004). Climatologically, the altitude of the tropopause represents the seasonal variation of the flux of stratospheric air intruding into the troposphere (Appenzeller et al., 1996). Moreover, the tropopause

height trends can be a sensitive indicator of anthropogenic climate change (Sausen and Santer, 2003; Santer et al., 2003a; Añel et al., 2006).

A variety of ways are available to determine the extratropical tropopause. Radiosonde sounding is the most commonly used to define the thermal tropopause (hereafter referred to as LRT) based on temperature lapse-rate (WMO, 1957). The thermal definition of tropopause can be applied globally and the tropopause height easily be determined from one individual profile (Santer et al., 2003). Another feasible definition is to use a specific potential vorticity (PV) surface to represent the dynamical tropopause (hereafter referred to as PVT) (Reed, 1955; Hoskins et al., 1985). Dynamical definition has the advantage that the PV is a conserved property (under adiabatic and friction-less conditions) of an air mass (Hoskins et al., 1985; Bethan et al., 1996). Values in the range 1-4 PVU (1 PVU=$10^6 \mathrm{m}^2 s^{-1} K kg^{-1}$) are used in previous researches in the Northern Hemisphere (e.g. Baray et al., 2000; Sprenger et al., 2003; Hoerling et al., 1991). The threshold of 2 PVU surface is the most commonly used (Gettelman et al., 2011). Dynamical definition, however, is not applicable near the equator, where the PV tends to be 0 (e.g., Hoerling et al., 1991; Nielsen-Gammon et al., 2001). Creating a blended tropopause globally may probably a good way forward (Wilcox et al., 2011). In addition, the data of GPS radio occultation satellites is also an effective way and commonly applied to study tropopause (e.g. Schmidt et al., 2005; Son et al., 2011).

As a result of partial specular reflection from stable atmospheric layer, the radar tropopause (RT) can be well represented and identified by atmospheric radars operating at meter wavelength (VHF band) and directing at vertical incidence (Gage and Green,

1979). Research activity increased remarkably following the first report on VHF radar detection of tropopause by Gage and Green (1979), for instance, the researches in middle latitudes (e.g. Hermawan et al., 1998), polar regions (e.g. Hall, 2013a), and tropical regions (e.g. Das et al., 2008; Ravindrababu et al., 2014). Several methods have been proposed to determine the tropopause height via radar echo power, including the largest gradient in echo power (Vaughan et al., 1995; –Alexander et al., 2013), the maximum echo power (Vaughan et al., 1995; Hall et al., 2009), and the specific value of echo power (Gage and Green, 1982; Yamamoto et al., 2003). The method of the RT height determination used in this paper will be described in detail in next section.

The biggest advantage of ~~the~~ VHF radar measurements is the ability of continuous operation unmanned in any weather conditions. Of course, no definition of the tropopause is perfect. VHF radar system can only be limited to a few locations globally. A detailed review of the close relationship between these different tropopause definitions is provided by Alexander et al., (2012).

By means of the radiosonde, reanalysis, and satellite data available globally, long-term (annual or longer) variability in tropopause height has received extensive attention (e.g. Randel et al., 2000; Angell and Korshover, 2009; Son et al., 2011; Liu et al., 2014). However, short period (diurnal or semidiurnal) variability of the tropopause is hard to be examined by these measurements. In contrast, benefiting from the much higher temporal resolution, radar definition of the tropopause provides good capability for studying the diurnal and semidiurnal variation in tropopause height. Earlier, Yamamoto et al., (2003) reported the capability of the Equatorial Atmospheric Radar to examine

the diurnal variation of tropopause height. Then, the diurnal variability of the tropical tropopause was investigated in detail by Das et al., (2008) using the Indian Gadanki MST radar. Its diurnal variation over a polar latitude station was investigated by Hall (2013b). In the absence of pressure and temperature parameters, the evidence of atmospheric tides can be well represented by winds (e.g. Huang et al., 2015).

The tropopause structure in midlatitudes is different from that in other regions. Double tropopauses structure is a ubiquitous feature over mid-latitude regions near 40°N (Pan et al., 2004; Randel et al., 2007). Strong evidence has revealed that the poleward intrusion of subtropical tropospheric air that occurred above the subtropical jet have resulted in the double structure (Pan et al., 2009). The higher part (second tropopause near ~16 km) is characterized by tropical features of cold and higher level, whereas the lower part (first tropopause near ~12 km) is characterized by polar features of warm and lower level. In the present study, we focus only on the first tropopauses ~~(~~below 16 km~~, if it exists) which~~ and these will be referred to as 'tropopause' hereafter.

In this study, using more than 5 years of Beijing MST radar echo power measurements in vertical beam, we mainly focus on the high-resolution characteristics of the tropopause structure and their comparison with the simultaneous radiosonde and dynamical definitions. Another important objective of this study is to examine the diurnal and semidiurnal variability of the tropopause. The observational characteristics of e.g. winds, echo power, and data acquisition rate near the tropopause layer are also presented in the paper.

2. Data and Methods

2.1. Radar Dataset

As an important part of the Chinese Meridian Project, two MST radar systems are designed and constructed to improve the understanding of the extratropical troposphere, lower stratosphere, and mesosphere (Wang, 2010), which are Wuhan and Beijing MST radars. The Beijing MST radar located in Xianghe, Hebei Province, China (39.75° N, 116.96° E, 22 m above sea level) was designed and constructed by the Institute of Atmospheric Physics, Chinese Academy of Sciences and started its routine operation since 20 October 2011 (Tian and Lu, 2017). The radar is a high power coherent pulse-Doppler radar operating at 50 MHz with the maximum peak power of 172 kW and the half-power beam width of 3.2°. Five beams are applied: one vertically pointed beam and four 15° off-zenith beams tilted to north, east, south, and west. In order to obtain the high-quality measurements from troposphere, lower stratosphere, and mesosphere simultaneously, the radar is designed to operate routinely in three separate modes: low mode (designed range 2.5-~12 km), middle mode (10-~25 km), and high mode (60-~90 km) with vertical resolutions of 150, 600, and 1200 m, respectively. Under the routine operation, the 15-min break is followed by the 15-min operation cycle (5 min for each mode). As a result, the time resolutions of the low, middle, and high mode measurements are all 30 min. More detailed review of the radar system is given by Chen et al. (2016).

Here only the low mode echo power measurements are used to determine the RT height. Although the designed detectable range of the low mode is from 2.5-~12 km,

the vertically pointed beam can receive stronger echoes from a higher level (~14-15 km) as compared with those from off-vertical beams due to the partial specular reflection mechanism. The measurements in middle mode are ~~also~~ applied to calculate the winds or echo power within ~5-6 km of the tropopause. The parameters for the two routine operation modes are listed in Table 1. The monthly total number of the echo power profiles available in vertical beam (low mode) is shown in Fig. 1. The outliers or severely contaminated data that mainly induced by system problems are eliminated. The large data gap in September is due to the annual preventive maintenance.

2.2. Tropopause Definitions

~~D~~ue to the large gradient in potential temperature, radar return power received at vertical incidence is significantly enhanced upon the transition zone of the tropopause layer. Using this characteristic, the RT height can be determined effectively ~~by the VHF radar~~. Here, the RT is defined as the altitude (above 500 hPa) where the maximum vertical gradient of echo power is located (Vaughan et al., 1995; –Alexander et al., 2013; Ravindrababu et al., 2014; Chen et al., 2018). Considering the occasional and random noise, to which the derived-RT is sensitive, the echo power profiles are smoothed by a 3-point running mean. In order to further reduce the influence of the noise, the RT definition used here need to satisfy an additional criterion: the determined RT height should be continuous with the adjacent RT heights (one on each side), otherwise to search for the second peak gradient (eliminated if the second peak does not meet the additional criterion). The “continuous” here means that the discrepancy between the two successive heights (in time, 0.5-hour interval) should be <0.6 km. A

typical example of the RT and LRT is illustrated in Fig. 2. The LRT is identified based on the World Meteorological Organization (WMO) criteria (WMO, 1957). The radar aspect sensitivity is expressed as the ratio between vertical (p_v) and oblique (p_o) beam (here is 15° east beam) echo power ~~(here is 15° east beam)~~. The radiosonde soundings are launched twice daily from the Beijing Meteorological Observatory (39.93 °N, 116.28 °E, station number 54511), which is less than 45 km to the radar site. In this case, the LRT and RT consistent well and are at 11.65 km and 11.85 km respectively. As expected, the LRT characterized by a rapid increase in potential temperature gradient also corresponds to ~~the~~ large gradient in radar aspect sensitivity. Note that the height with maximum value in echo power lie at a higher altitude ~~(as compared with the~~than that of the RT~~, height)~~ of ~700 m above the LRT. The dynamical tropopauses used in this paper are derived from the European Centre for Medium-Range Weather Forecasts (ECMWF) ERA-Interim Reanalysis (Dee et al., 2011) and defined as the surface of 2 PVU potential vorticity, which is same to that used by Sprenger et al., (2003) and Alexander et al. (2013).

2.3. Tropopause sharpness definition

For the compared data pairs between the RT and LRT, we calculate the corresponding tropopause sharpness that represents the strength of the tropopause inversion layer. As defined by Wirth, (2000), the tropopause sharpness S_{TP} can be calculated as:

$$S_{TP} = \frac{T_{TP+\Delta Z} - T_{TP}}{\Delta Z} - \frac{T_{TP} - T_{TP-\Delta Z}}{\Delta Z} \quad (1)$$

where TP denotes the tropopause height, $\Delta Z = 1$ km, and T_{TP} indicates the

corresponding temperature. This definition is also used in Alexander et al. 2013 and we're using it for a good comparison with our results.

3. Results

3.1. High-resolution radar tropopause structure

The height-time cross section of radar echo power and aspect sensitivity is shown in Fig. 3 for a typical month (February 2014), along with the RT, PVT and LRT marked in the figure. ~~In general, t~~The RT agreed well with both the LRT and PVT in height, and most of the RT exhibit a slightly higher altitude. However, the differences between the RT and LRT are sometimes large (reach to ~1-2 km)~~–~~, especially when the RT experience rapid change. Regardless of the background synoptic condition, the difference in the definitions themselves is to a large degree the main contributing factor for the large difference between the RT and LRT. For example, a second layer with significant enhanced echo power is observed above the radar-derived RT for the cases on 4 and 5 February 2012 (Fig.3a). According to the definitions, the RT is well defined as the first layer with enhanced echo power and the LRT matched the second layer, similar to that observed by Yamamoto et al., (2003) and Fukao et al., (2003). It is of note that the RT well separates the troposphere characterized by low aspect sensitivity from the lower-stratosphere characterized by high aspect sensitivity (Fig.3b).

3.2. Comparisons between different definitions

To further quantify the consistency and difference in altitude between different tropopause definitions, a detailed comparison is carried out in this section. The seasonal scatterplots for RT versus LRT and the histogram distribution of altitude differences

between ~~the RT and LRT~~them are ~~illustrated~~ shown in Fig. 4, ~~during~~ for the period November 2011-May 2017. A total of 2411 data pairs are obtained for comparison. Among them, the number of data pairs is 845 for DJF (winter), 721 for MAM (spring), 321 for JJA (summer), and 524 for SON (autumn). Comparisons have shown a good consistency throughout the seasons and most of the RTs exhibit a slightly higher than the LRTs. The correlation coefficient is 0.74, 0.80, 0.82, and 0.78 for DJF, MAM, JJA, and SON, respectively. The mean and standard deviation difference (RT minus LRT) calculated in DJF, MAM, JJA, and SON is (0.14±0.75), (0.26±0.78), (0.33±0.56), and (0.12±0.69) km, respectively. The proportion of the data pairs with differences <500 m is reasonably good during four seasons and is 63%, 61%, 64%, and 67% for DJF, MAM, JJA, and SON, respectively. Results of Fig. 4 ~~explicitly shows that the RT derived by the~~indicate the potential of Beijing MST radar ~~agrees reasonably well with the LRT~~for detecting tropopauses throughout the seasons.

To examine the potential role of the sharpness, Fig. 5a and Fig. 5b show the histogram distribution of the tropopause sharpness along with the probability density curve for data pairs with difference (absolute values of RT minus LRT) <0.5 km and >1 km respectively. ~~What is apparent is~~Results indicate that higher probabilities of large tropopause sharpness values occur when the RT-LRT difference is less than 0.5 km~~most data pairs of Fig. 5a are located to the right (higher sharpness values, with the peak of ~7.06 K/km) and of Fig. 5b are to the left (lower sharpness values, with the peak of ~6.35 K/km)~~. No matter whether this distribution feature is associated with the cyclonic-anticyclonic systems (e.g. Randel et al., 2007; Randel and Wu, 2010), the

results more or less demonstrate that the larger (weaker) tropopause sharpness contribute to lower (higher) difference between the RT and LRT. From the perspective of seasonal statistics, the tropopause sharpness over Beijing station shows similar distribution characteristics throughout the seasons (not shown), which is different from that in polar regions where the sharpness is significantly higher during summer than during winter (Zängl and Hoinka, 2001).

The seasonal scatterplots and height difference histograms ~~distribution~~ between the RT and PVT are illustrated and quantified in Fig. 6. The total number of comparing data pairs for winter, spring, summer, and autumn is 1422, 1260, 791, and 1145, respectively. During winter and spring (Fig. 6a and 6b), the RTs agree reasonably well with the PVTs with the correlation coefficient of 0.72 and 0.76 and the mean difference (RT minus PVT) of (0.55±0.84 km) and (1±0.89 km), respectively. In contrast, the consistency for summer and autumn (Fig. 6c and 6d) is relatively bad and with correlation coefficient of 0.33 and 0.47 and mean difference of (0.80±1.39 km) and (0.75±1.23 km), respectively. Especially for summer, the proportion of the comparing data pairs with difference <0.5 km is only 10.6% (84). ~~In autumn, need to note that most data pairs with poor consistency is sampled during early autumn.~~

3.3. Observational characteristics in the vicinity of tropopause

M~~easurements of radar m~~Middle mode radar measurements are used for examining the horizontal wind, return power, and effective wind data acquisition rate within 5-6 km of the tropopause (upper troposphere and lower stratosphere). Left panels of Fig. 7 show the vertical scatterplots of the static stability (represented by the

buoyancy frequency squared) as a function of height relative to the LRT and ~~the~~ right panels show the radar echo power as a function of height relative to the RT, during two specific years 2012-2013 for extended winter NDJFM and summer MJJAS seasons. Mean and standard deviations are also plotted in each panel of Fig. 7. ~~As expected,~~ ~~r~~Results clearly show sudden jump in static stability and radar power near the tropopause layer. The ~~degree of~~ sudden increase in echo power is more gradual than that in static stability. The amplitude of the sudden increase in radar power experienced a slightly larger during NDJFM than that during MJJAS (red lines of right panels). Another interesting feature in the lower-stratosphere is that ~~both~~ the static stability ~~and radar power points~~ show less disperse during NDJFM than that during MJJAS.

Fig. 8 shows the profiles of mean ~~radar effective wind~~ data acquisition rate in radar wind for low and middle modes during November 2011-May 2017. ~~Clearly, b~~Both profiles exhibit a sudden increase with height near the tropopause, with the first peak located ~1 km higher above the mean tropopause height. Note that the second inversion in middle mode profile that occurred near 16 km is associated with the second tropopause. As limited by the highest detectable altitude (the data acquisition rate decreased to lower than 20% at ~16 km), the profile in low mode shows little evidence of second inversion.

Fig. 9 shows time-height intensity plot of the monthly mean radar-derived horizontal wind ~~(from middle mode)~~ during November 2011-May 2017, together with the monthly mean location of RT and LRT. ~~One pixel grid denotes 1 month×0.6 km.~~ The monthly mean RT and LRT agreed well with each other in height, within 400 m in

August and September and even lower in other months of about within 200 m. They both exhibit a clear seasonal variation, with maximum in early autumn of ~11.6 km and minimum in early spring of ~10.3 km. The monthly mean wind jet varies with season, with the thinnest thickness and lowest strength in summer. The mean tropopause height ~~appears to~~ corresponds to the lower boundary location of peak wind layer. The error bars of both the RT and LRT help to illustrate that the tropopauses changes by larger amplitude in winter and June than that in other months.

3.4. Periodogram analysis of the radar tropopause

High temporal resolution detection of tropopause by VHF radar have allowed us to investigate the diurnal or semidiurnal variability of the tropopause. Atmospheric tides are well known global oscillations contributing to the diurnal variation in temperature and background winds, which in turn modulate the tropopause height. With the absence of temperature measurements, zonal and meridional winds are applied to demonstrate the evidence of diurnal or semidiurnal modulation by tidal. The frequency power spectrum of the RT height, zonal and meridional wind, calculated by means of Lomb-Scargle method (Press and Rybicki, 1989), is illustrated in Fig. 10 for two typical months: May 2015 and December 2016. ~~The choice of~~ Lomb-Scargle algorithm is applied due to the presence of data gaps (~2 days per week, especially during 2012-2013). The dominant ~24 h periodicity in all the three parameters ~~in RT height, zonal and meridional wind~~ is obvious for both months. The evidence of ~12 h period ~~in all three parameters~~ is ~~distinct~~ observed for May 2015 (Fig. 10a), although the power is relatively weaker. Through the analysis for each individual month, we found that the

semidiurnal component in the three parameters is generally and occasionally observed in summer and later spring during our experimental period. ~~The c~~Characteristics of the diurnal variation ~~of the~~in RT height can be better represented ~~better~~ in Fig. 11, which shows the mean Lomb-Scargle power spectrum of the RT as a function of month during November 2011-May 2017. As compared with other months, the dominant diurnal periodicity is less evident in April. We need to clarify that atmospheric tides are of course not the only source of the diurnal variation in tropopause height, diurnal convective activities (Yamamoto et al., 2003) might also be an important cause. Here will not be discussed in detail.

4. Discussion

As for the radar echo power definition, the RT estimation sometimes will fail due to the system problems, even if the thermal tropopause is well defined (Hall et al., 2009). Apart from the system problems (e.g. the damage of T/R module), the following two conditions are primarily responsible for the failure (or difficulty) of both the radar and thermal definitions over the radar site latitude (~40° N). Firstly, the temperature sometimes continued to decrease until to the stratosphere (above 16 km) in summer and early autumn, leading to the failure/difficulty of both the radar and thermal definitions (a typical case as shown in Fig. 12a). Need to note that the temperature inversion layer occurred at ~16 km in summer or early autumn is the second tropopause with characteristics of Tropics (Pan et al., 2004; Randel et al., 2007). Secondly, some specific meteorological processes can lead to the ambiguities and indefiniteness in thermal and

radar definitions, such as fronts, cyclones or typhoons, and folding (e.g. Nastrom et al., 1989; May et al., 1991; Roettger, 2001; Alexander et al., 2013). Such ambiguities often result in large difference in altitude between the RT and LRT. ~~In addition, when multiple temperature inversion layers occurred (below 16 km), the RT sometimes matched the lower layer with enhanced echo power and LRT often matched the upper layer (e.g. Yamamoto et al., 2003; Fukao et al., 2003).~~ Apart from the situations above, another condition is also commonly responsible for the difficult in identifying the thermal tropopause from radiosonde profiles during summer. As a typical case shown in Fig. 12b, a significant inversion in temperature (at ~12 km) is recorded from the radiosonde profile, but the altitude extent of inversion layer is too thin to meet the WMO criterion that thermal definition required. Whereas, the apparent enhancement in radar echo power corresponding to such inversion layer is strong enough to well define the RT. The temperature inversion located near ~16 km (the second tropopause) is not the focus of this paper.

Pan et al., (2004) have reported that the difference between the LRT and PVT are more distinct in the vicinity of subtropical jet. In the northern hemisphere, the axis of the subtropical jet is situated near ~30°N in spring and winter, whereas in summer and early autumn the subtropical jet shifts northward to ~40°N (see Fig. 4 in Ding and Wang, 2006). We preliminary considered that the inconsistency between the RT and PVT in summer and early autumn (Fig. 6c and 6d) is most likely related to the subtropical jet shifting poleward to ~40°N. The existing cyclones or anticyclones in the upper-troposphere (Wirth, 2000), of course, may also be an important influence factor for the

significant asymmetric differences (most of the scattered points deviate significantly from the 1:1 line). The asymmetric differences, that is most of the RT are located higher than the 2PVU tropopause height, suggest that the 2PVU surface is not the best measure of a dynamical tropopause over Beijing during summer-time. More detailed discussion about the striking asymmetric differences in height between LRT and PVT can be seen in Wirth (2001) and will not be given here. Anyway, we need to be careful when using the 2PVU dynamical definition to define the tropopause over radar site latitude ~40° N, especially in summer.

About the characteristics of tropopause and the comparison between different definitions, there are many differences between mid-latitude and polar regions. In mid-latitude (~40°N), our results show that: (1) the agreement between RT and LRT is similar good throughout the seasons; (2) RTs are generally located higher than the LRT; (3) the thermal definition sometimes fail in summer and early autumn; (4) the agreement between the RT/LRT and PVT in summer is poor. Whereas, in contrast, previous researches about the tropopause over polar regions reported that (Wirth, 2000；Alexander et al., 2013): (1) the difference between the RT and LRT is larger during winter than that during summer; (2) RTs are generally located lower than the LRT; (3) the thermal definition sometimes fail in winter and spring; (4) the comparison between the RT and PVT showed the similar good agreement during both summer and winter.

Over a polar latitude station, the seasonal characteristics of the diurnal oscillation in tropopause height were investigated using 5 years of SOUSY VHF radar measurements (Hall, 2013b). The sunlight variability in polar regions is different from

354 that in other latitudes of the world. Different sunlight variation actually will lead to
355 difference in atmospheric tides, and then would result in different diurnal variation in
356 tropopause height. Here we found that the diurnal oscillation of RT height at Xianghe
357 is ubiquitous and obvious throughout the seasons except for April (Fig. 11). Whereas at
358 polar latitude and in months of November to February when there is no sunlight, Hall
359 (2013b) observed little evidence of 24 h diurnal variability in RT height.
360
361 **5. Conclusions**
362 In this paper, we present the high resolution structure and variability of the
363 tropopause in Xianghe, China (39.75° N, 116.96° E), based on the Beijing MST radar
364 vertical beam echo power data collected during the period November 2011-May 2017.
365 Fine-scale structure of the RT is well determined with a high temporal resolution of 0.5
366 h. Comparison results have shown good agreement in altitude between the RT and LRT,
367 with a correlation coefficient of ≥ 0.74 for the four seasons. Higher tropopause
368 sharpness seems to contribute lower difference between the RT and LRT in altitude and
369 weaker sharpness appears responsible for higher difference. The agreement between the
370 RT and PVT is relatively well in winter and spring with correlation coefficient of 0.72
371 and 0.76 respectively, but poor during summer with a correlation coefficient of only
372 0.33. We initially suggested that the poor consistency between RT and PVT is associated
373 with the subtropical jet shifting poleward to ~40°N.
374 As expected, the sudden jump in static stability (represented by the buoyancy
375 frequency squared) and the rapid increase in radar echo power upon the tropopause

layer are clearly observed. Upon the tropopause layer, a sudden increase in effective radar data acquisition rate is also observed. Both the monthly mean RT and LRT height have shown a clear ~~annual~~ seasonal ~~cycle~~variation. The variability and oscillation of RT height with diurnal or lower timescales is presented. Obvious diurnal variation in tropopause height, zonal wind, and meridional wind is generally observed throughout the seasons, indicating the modulation most likely from the atmospheric tides. The semidiurnal variation in RT height is not so obvious and commonly observed occasionally in summer and late spring.

Data availability. MST radar data are publicly and freely avail- able at http://159.226.22.74/ (MST, 2019). ECMWF ERA-interim data are publicly and freely available at https://www.ecmwf.int/en/forecasts/datasets (ECMWF, 2019). Global radiosonde data are publicly available from the NOAA/ESRL Database at https://ruc.noaa.gov/raobs/ (Radiosonde, 2019).

Author contributions. FC originally conceived and designed the study, in consultation with GC. The processing and data analysis for radar, radiosonde, and reanalysis data was developed by FC. GC, YT, SZ, and KH are the people in charge of MST radar data archiving, mage-generation and quality control. CW and WZ helped to check the manuscript.

~~A~~**cknowledgment**. –

This work is funded by National Natural Science Foundation of China (NSFC grants No. 41474132 and 41722404). We acknowledge the Chinese Meridian Project for providing the MST radar data. The authors sincerely acknowledge the ECMWF for providing global reanalysis data. ~~The MST radar data for this paper are available at Data Centre for Meridian Space Weather Monitoring Project (http://159.226.22.74/). The radiosonde data are publicly available from the NOAA/ESRL Database at https://ruc.noaa.gov/raobs/.~~

References

Alexander, S.P., Murphy, D.J., and Klekociuk, A.R.: High resolution VHF radar measurements of tropopause structure and variability at Davis, Antarctica (69◦ S, 78◦ E), Atmos. Chem. Phys., 13, 3121-3132, 2013.

Angell, J. K., and Korshover, J.: Quasi-biennial and long-term fluctuations in tropopause pressure and temperature, and the relation to stratospheric water vapor content. Monthly Weather Review, 102(1), 29-34, 2009.

Appenzeller, C., Holton, J. R., and Rosenlof, K. H.: Seasonal Variation of Mass Transport Across the Tropopause. Journal of Geophysical Research, 101(D10), 15071-15078, 1996.

Añel, J. A., J. C. Antuña, L. de la Torre, R. Nieto, and Gimeno L.: Changes in tropopause height for the Eurasian region determined from CARDS radiosonde data. Naturwissenschafte, 93, 603–609, doi:10.1007/s00114-006-0147-5, 2006.

Bethan, S., Vaughan, G., and Reid, S. J.: A comparison of ozone and thermal tropopause

420 heights and the impact of tropopause definition on quantifying the ozone content
421 of the troposphere. Quarterly Journal of the Royal Meteorological Society,
422 122(532), 929-944, 1996.
423 Baray, J., Daniel, V., Ancellet, G., and Legras, B.: Planetary-scale tropopause folds in
424 the southern subtropics. Geophysical Research Letters, 27(3), 353-356, 2000.
425 Chen, F. L., Chen, G., Shi, C. H., Tian, Y. F., Zhang, S. D., and Huang, K. M.: Strong
426 downdrafts preceding rapid tropopause ascent and their potential to identify cross-
427 tropopause stratospheric intrusions, Annales Geophysicae, 36(5), 1403-1417,
428 2018.
429 Chen, G., Cui, X., Chen, F., Zhao, Z., Wang, Y., Yao, Q., and Gong, W.: MST Radars
430 of Chinese Meridian Project: System Description and Atmospheric Wind
431 Measurement. IEEE Transactions on Geoscience and Remote Sensing, 54(8),
432 4513-4523, 2016.
433 Das, S. S., Jain, A. R., Kumar, K. K., and Rao, D. N.: Diurnal variability of the tropical
434 tropopause: Significance of VHF radar measurements. Radio Science, 43(6), 1-14,
435 doi:10.1029/2008RS003824, 2008.
436 Dee, D. P., Uppala, S. M., Simmons, A. J., Berrisford, P., Poli, P., Kobayashi, S. et al.:
437 The ERA-Interim reanalysis: configuration and performance of the data
438 assimilation system. Quarterly Journal of the Royal Meteorological Society,
439 137(656), 553-597, 2011.
440 Ding, A., and Wang, T.: Influence of stratosphere-to-troposphere exchange on the
441 seasonal cycle of surface ozone at Mount Waliguan in western China. Geophysical

442 Research Letters, 33(3), 233-252, doi:10.1029/ 2005GL024760, 2006.
443 Fukao, S., H. Hashiguchi, M. Yamamoto, T. Tsuda, T. Nakamura, M. K. Yamamoto,
444 T. Sato, M. Hagio, and Y. Yabugaki:. Equatorial Atmosphere Radar (EAR):
445 System description and first results. Radio Science, 38(3), 1053, 2003.
446 Gage, K. S., and Green, J. L.: An objective method for the determination of tropopause
447 height from VHF radar observations. Journal of Applied Meteorology, 21(21),
448 1150-1154, 1982.
449 Gage, K. S., and Green, J. L.: Tropopause Detection by Partial Specular Reflection with
450 Very-High-Frequency Radar. Science, 203(4386), 1238-1240, 1979.
451 Gettelman, A., P. Hoor, L. L. Pan, W. J. Randel, M. I. Hegglin, and T. Birner: The
452 extratropical upper troposphere and lower stratosphere, Reviews of Geophysics,
453 49(3), RG3003, doi: 10.1029/2011RG000355, 2011.
454 Hermawan, E., Tsuda, T., and Adachi, T.: MU radar observations of tropopause
455 variations by using clear air echo characteristics. Earth, Planets and Space, 50(4),
456 361-370, 1998.
457 Hall, C.: The radar tropopause above Svalbard 2008–2012: Characteristics at various
458 timescales. Journal of Geophysical Research, 118(6), 2600-2608, 2013a.
459 Hall, C.: The radar tropopause at 78°N, 16°E: Characteristics of diurnal variation.
460 Journal of Geophysical Research, 118(12), 6354-6359, doi:10.1002/jgrd.50560,
461 2013b.

462 Hall, C. M., Röttger, J., Kuyeng, K., Sigernes, F., Claes, S., and Chau, J. L.: Tropopause
463 altitude detection at 78°N, 16°E, 2008: First results of the refurbished SOUSY
464 radar. Radio Science, 44(5), 1-12, doi:10.1029/ 2009RS004144, 2009.
465 Hoinka, K. P.: Statistics of the Global Tropopause Pressure. Monthly Weather Review,
466 126(12), 3303-3325, 1998.
467 Hoskins, B. J., Mcintyre, M. E., and Robertson, A. W.: On the use and significance of
468 isentropic potential vorticity maps. Quarterly Journal of the Royal Meteorological
469 Society, 111(470), 877-946, 2007.
470 Huang, C., Zhang, S. D., Zhou, Q. H., Yi, F., Huang, K., Gong, Y., Zhang, Y., and Gan,
471 Q.: WHU VHF radar observations of the diurnal tide and its variability in the lower
472 atmosphere over Chongyang (114.14° E, 29.53° N), China. Annales Geophysicae,
473 33(7), 865-874, 2015.
474 Hoerling, M. P., Schaack, T. K., and Lenzen, A. J.: Global Objective Tropopause
475 Analysis. Monthly Weather Review, 119(8), 1816-1831, 1991.
476 Liu, Y., Xu, T., and Liu, J.: Characteristics of the seasonal variation of the global
477 tropopause revealed by cosmic/GPS data. Advances in Space Research, 54(11),
478 2274-2285, 2014.
479 May, P. T., Yamamoto, M., Fukao, S., Sato, T., Kato, S., and Tsuda, T.: Wind and
480 reflectivity fields around fronts observed with a VHF radar. Radio Science, 26(5),
481 1245-1249, 1991.

Nastrom, G. D., Green, J. L., Gage, K. S., and Peterson, M. R.: Tropopause Folding and the Variability of the Tropopause Height as Seen by the Flatland VHF Radar. Journal of Applied Meteorology, 28(12), 1271-1281, 1989.

Nielsen-Gammon, J. W.: A visualization of the global dynamic tropopause. Bulletin of the American Meteorological Society, 82(6), 1151-1168, 2001.

Pan, L. L., Randel, W. J., Gary, B. L., Mahoney, M. J., and Hintsa, E. J.: Definitions and sharpness of the extratropical tropopause: A trace gas perspective. Journal of Geophysical Research, 109, D23103, doi:10.1029/2004JD004982, 2004.

Pan, L. L., W. J. Randel, J. C. Gille, W. D. Hall, B. Nardi, S. Massie, V. Yudin, R. Khosravi, P. Konopka, and D. Tarasick: Tropospheric intrusions associated with the secondary tropopause, Journal of Geophysical Research, 114, D10302, 2009.

Press, W. H., and Rybicki, G. B.: Fast algorithm for spectral analysis of unevenly sampled data. The Astrophysical Journal, 338(1), 277-280, 1989.

Ravindrababu, S., Venkat Ratnam, M., Sunilkumar, S. V., Parameswaran, K., and Krishna Murthy, B. V.: Detection of tropopause altitude using Indian MST radar data and comparison with simultaneous radiosonde observations. Journal of Atmospheric and Solar-Terrestrial Physics, 121(6), 679-687, 2014.

Randel, W. J., Wu, F., and Gaffen, D. J.: Interannual variability of the tropical tropopause derived from radiosonde data and NCEP reanalyses. Journal of Geophysical Research Atmospheres, 105(D12), 15509-15523, 2000.

Randel, W. J., Seidel, D. J., and Pan, L. L.: Observational characteristics of double tropopauses. Journal of Geophysical Research, 112, D07309, 2007.

504 Randel, W. J., and Wu, F.: The Polar Summer Tropopause Inversion Layer. Journal of
505 the Atmospheric Sciences, 67(8), 2572-2581, 2010.
506 Randel, W. J., Wu, F., and Forster, P. M.: The extratropical tropopause inversion layer:
507 Global observations with GPS data, and a radiative forcing mechanism. Journal of
508 the Atmospheric Sciences, 64(12), 4489-4496, 2007.
509 Ramakrishnan, K. P.: Distortion of the tropopause due to meridional movements in the
510 sub-stratosphere. Nature, 132(3346), 932-932, 1933.
511 Roettger, J.: Observations of the polar d-region and the mesosphere with the Eiscat
512 Svalbard radar and the SOUSY Svalbard Radar (scientific paper). Memoirs of
513 National Institute of Polar Research. Special Issue, 54(94), 9-20, 2001.
514 Reed, R. J.: A study of a characteristic tpye of upper-level frontogenesis. Journal of the
515 Atmospheric Sciences, 12(3), 226-237, 1955.
516 Santer, B. D., Wehner, M. F., Wigley, T. M., Sausen, R., Meehl, G. A., Taylor, K. E.,
517 Ammann, C., Arblaster, J., Washington, W. M., Boyle, J. S., and Brüggemann, W.:
518 Contributions of anthropogenic and natural forcing to recent tropopause height
519 changes. Science, 301(5632), 479-483, 2003.
520 Santer, B. D., Sausen, R., Wigley, T. M., Boyle, J. S., Achutarao, K., Doutriaux, C.,
521 Hansen, J. E., Meehl, G. A., Roeckner, E., Ruedy, R., Schmidt, G., and Taylor, K.
522 E.: Behavior of tropopause height and atmospheric temperature in models,
523 reanalyses, and observations: Decadal changes. Journal of Geophysical Research,
524 108(D1), 4002, doi:10.1029/2002JD002258, 2003a.
525 Sausen, R., and Santer, B. D.: Use of Changes in Tropopause Height to Detect Human

526 Influences on Climate. Meteorologische Zeitschrift, 12(3), 131-136, 2003.
527 Schmidt, T., Heise, S., Wickert, J., Beyerle, G., & Reigber, C.: GPS radio occultation
528 with CHAMP and SAC-C: global monitoring of thermal tropopause parameters.
529 Atmospheric Chemistry and Physics, 5(6), 1473-1488, 2005.
530 Seidel, D. J., Ross, R. J., Angell, J. K., and Reid, G. C.: Climatological characteristics
531 of the tropical tropopause as revealed by radiosondes. Journal of Geophysical
532 Research, 106(D8), 7857-7878, 2001.
533 Son, S. W., Tandon, N. F., & Polvani, L. M.: The fine-scale structure of the global
534 tropopause derived from COSMIC GPS radio occultation measurements. Journal
535 of Geophysical Research: Atmospheres, 116(D20), 2011.
536 Sprenger, M., Croci Maspoli, M., and Wernli, H.: Tropopause folds and cross-
537 tropopause exchange: a global investigation based upon ECMWF analyses for the
538 time period March 2000 to February 2001. Journal of Geophysical Research
539 Atmospheres, 108(12), 291-302, 2003.
540 Tian, Y., and Lu, D.: Comparison of Beijing MST Radar and Radiosonde Horizontal
541 Wind Measurements. Advances in Atmospheric Sciences, 34(1), 39-53. doi:
542 10.1007 / s00376-016-6129-4, 2017.
543 Vaughan, G., Howells, A., and Price, J. D.: Use of MST radars to probe the mesoscale
544 structure of the tropopause. Tellus A, 47(5), 759-765, 1995.
545 Wang, C.: Development of the Chinese meridian project. Chinese Journal of Space
546 Science, 30(4), 382–384, 2010.
547 Wilcox L.J., Hoskins B.J., Shine K.P. 2012. A global blended tropopause based on ERA

548 data. Part I: Climatology. Q. J. R. Meteorol. Soc. 138: 561–575.
549 DOI:10.1002/qj.951.
550 Wirth, V.: Thermal versus dynamical tropopause in upper-tropospheric balanced flow
551 anomalies. Quarterly Journal of the Royal Meteorological Society, 126(562), 299-
552 317, 2000.
553 Wirth, V.: Cyclone-anticyclone asymmetry concerning the height of the thermal and the
554 dynamical tropopause. Journal of the Atmospheric Sciences, 58(1), 26-37, 2001.
555 WMO: Definition of the tropopause. WMO Bull., 6, 136, 1957.
556 Yamamoto, M., Oyamatsu, M., Horinouchi, T., Hashiguchi, H., and Fukao, S.: High
557 time resolution determination of the tropical tropopause by the Equatorial
558 Atmosphere Radar. Geophysical Research Letters, 30(21), 2094, 2003.
559 Zängl, G., and Hoinka, K. P.: The tropopause in the polar regions. Journal of Climate,
560 14(2001), 3117-3139, 2001.
561

562 **Table**

Radar parameter	Value
Transmitted frequency	50 MHz
Antenna array	24×24 3-element Yagi
Antenna gain	33 dB
Transmitter peak power	172 kW
Code	16-bit complementary
No. coherent integrations	128 (low mode)/64 (mid mode)
No. FFT points	256
No. spectral average	10
Pulse repetition period	160 (low mode)/320 (mid mode) μs
Half power beam width	3.2^o
Pulse length	1 (low mode)/4 (mid mode) μs
Range resolution	150 (low mode)/600 (mid mode) m
Temporal resolution	30 min
Off-zenith angle	15^o

563 **Table 1.** Routine operational parameters in low and middle mode for the Beijing MST
564 radar used in this study.

565

Figures

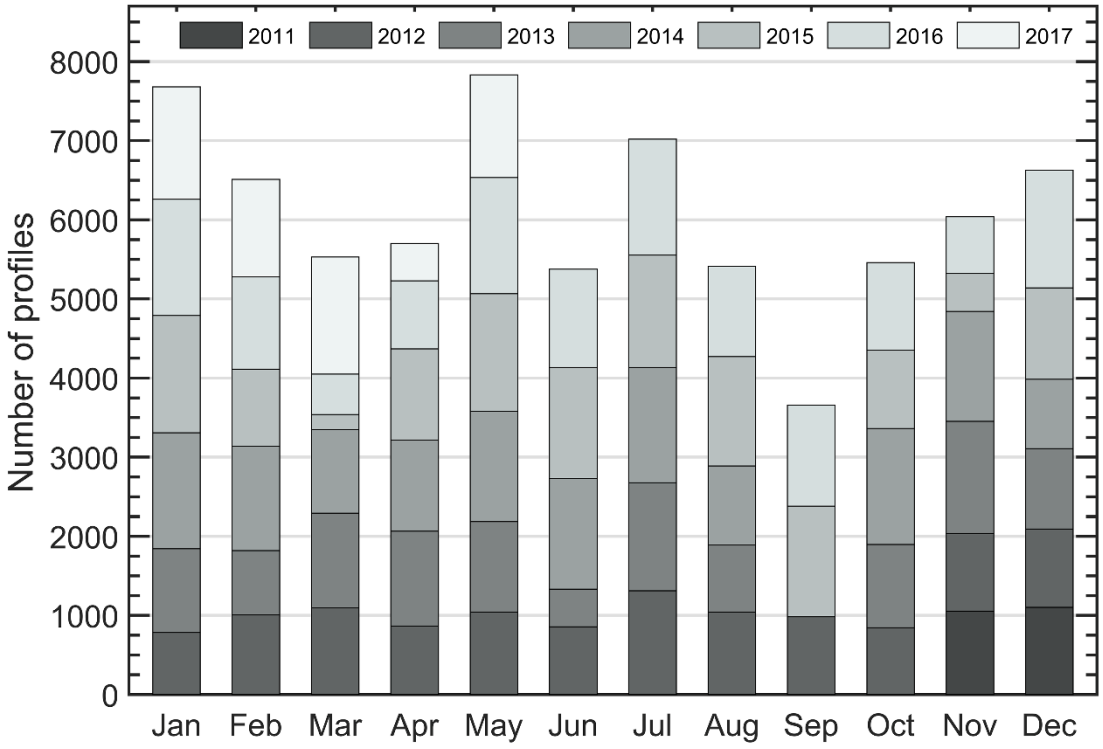

Figure 1. Distribution of the monthly total number of radar return echo power profiles that available from vertical beam in low mode, collected for the period November 2011-May 2017.

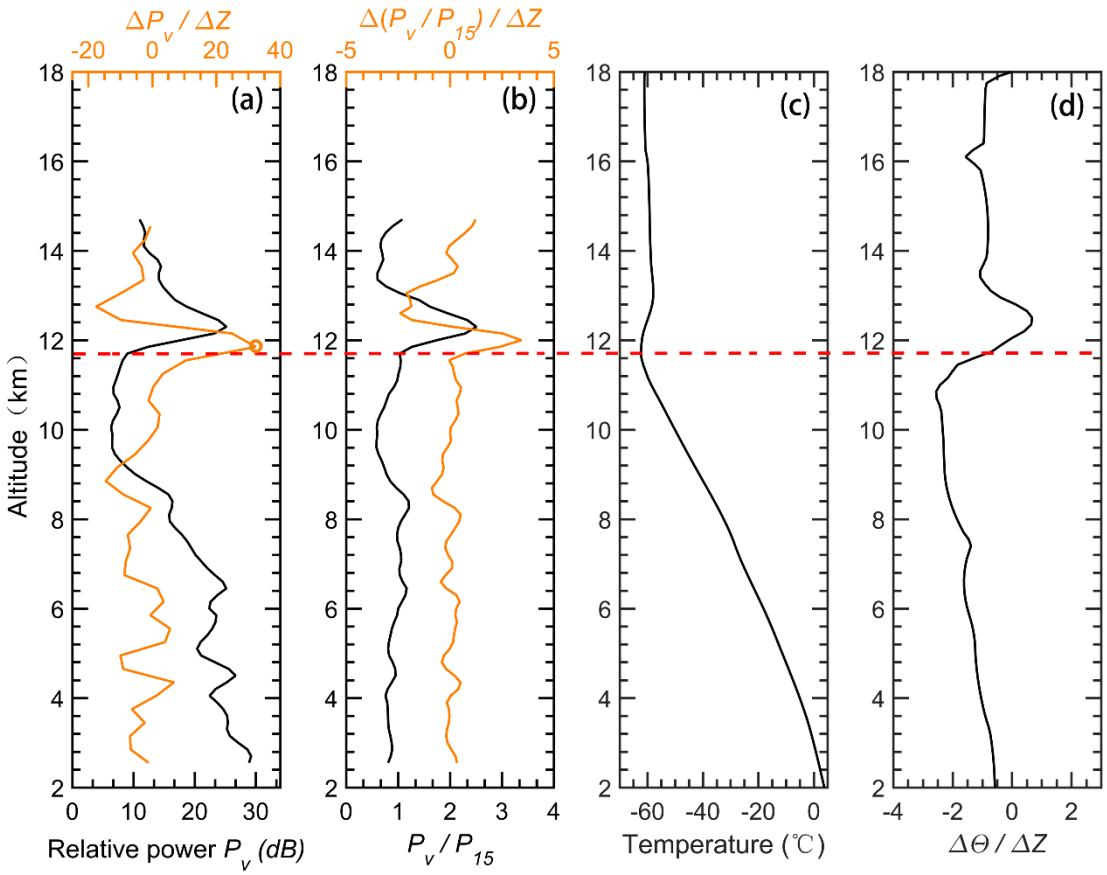

571

572 **Figure 2.** Example vertical profiles of (a) relative radar echo power (black line) along

573 with its gradient variation (orange line), (b) radar aspect sensitivity (black line) along

574 with its gradient variation (orange line), (c) radiosonde temperature and (d) potential

575 temperature gradient on 00 UT 04 November 2011. The horizontal red dashed line

576 marks the LRT height. The orange circle in ~~Fig. 2a~~(a) denotes the RT height.

577

578

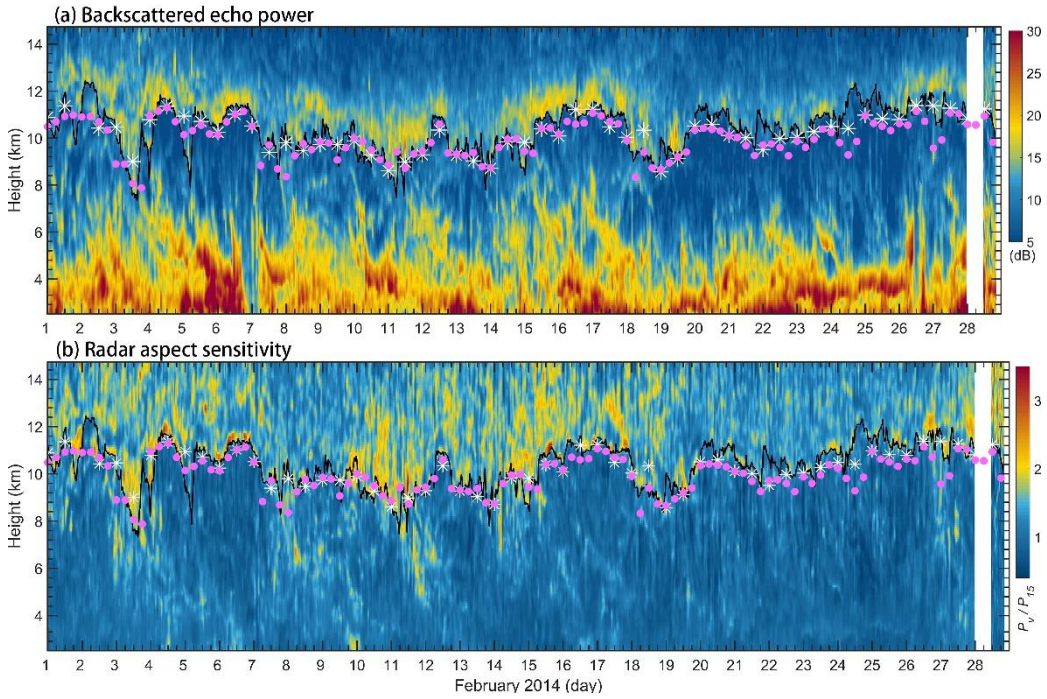

579

580 **Figure 3.** Altitude-time intensity plot of (a) radar backscattered echo power and (b)

581 radar aspect sensitivity for February 2014. The tropopauses determined based on the

582 radar echo definition are shown as a black solid curve. The ~~cyan~~ white asterisks '*' and

583 pink dots indicate the location of the LRT derived from simultaneous twice daily

584 radiosonde data and the PVT from ECMWF ERA-Interim reanalysis, respectively.

585 White stripe indicates the time frame of radar missing data.

586

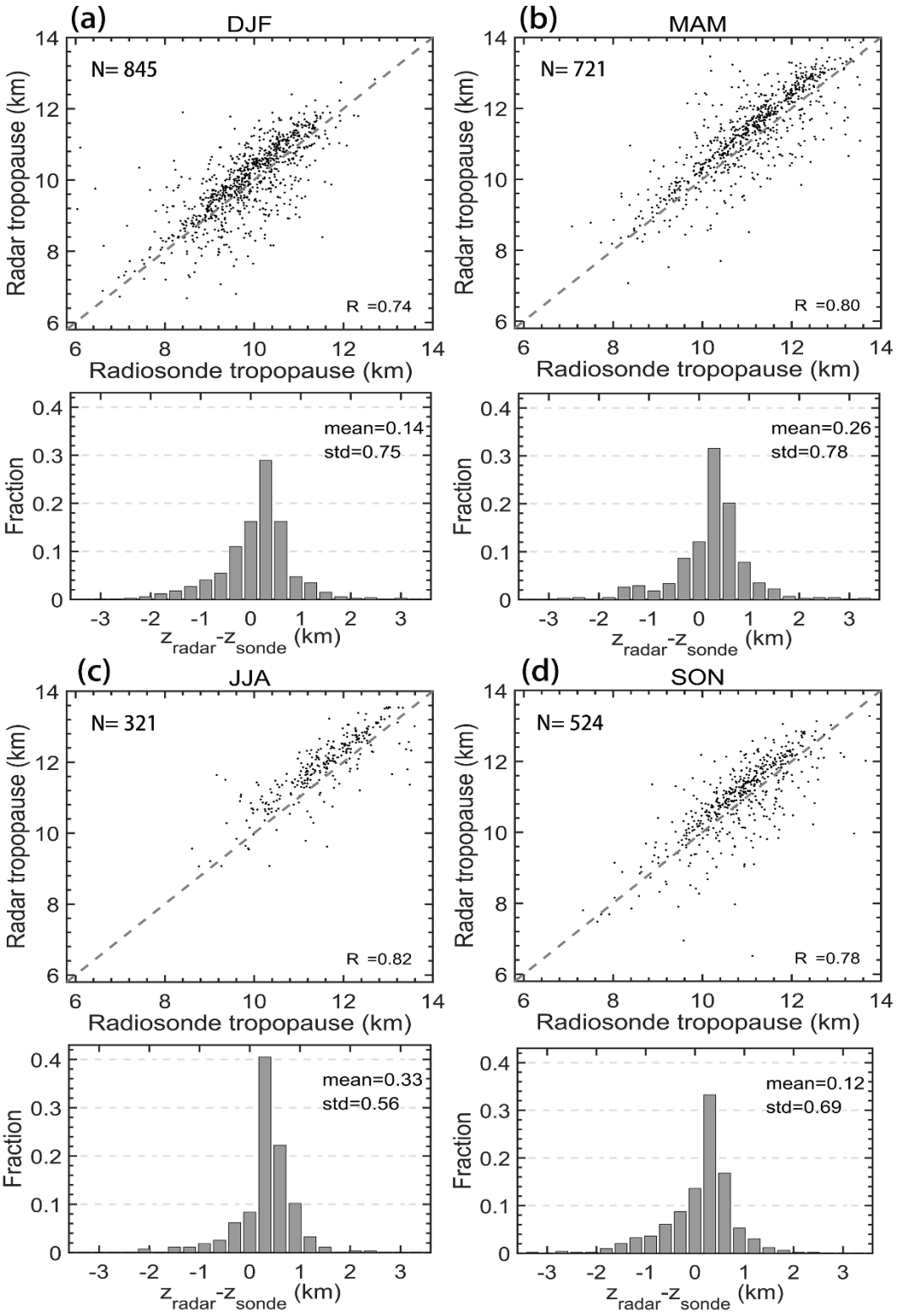

Figure 4. Seasonal scatterplots of the RT versus LRT and histogram distribution of altitude differences between the RT and the LRT, for (a) winter DJF, (b) spring MAM, (c) summer JJA, and (d) autumn SON, during the period November 2011-May 2017.

The positive values in the histogram indicate the RT locating at a higher level than the LRT. The grey dashed line shows the 1:1 line. Here, 'N','R^2', 'mean', and 'std' indicate the sample numbers, correlation coefficient, mean difference, and standard deviation of the difference, respectively.

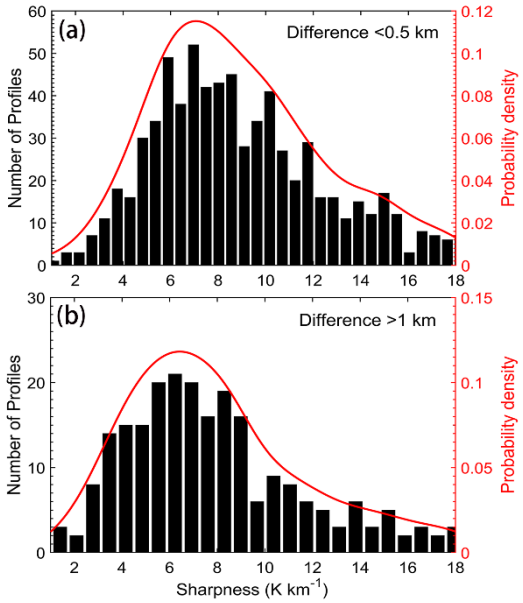

Figure 5. Histogram distribution of the tropopause sharpness for (a) difference <0.5 km, and (b) >1 km respectively between the LRT and the RT.

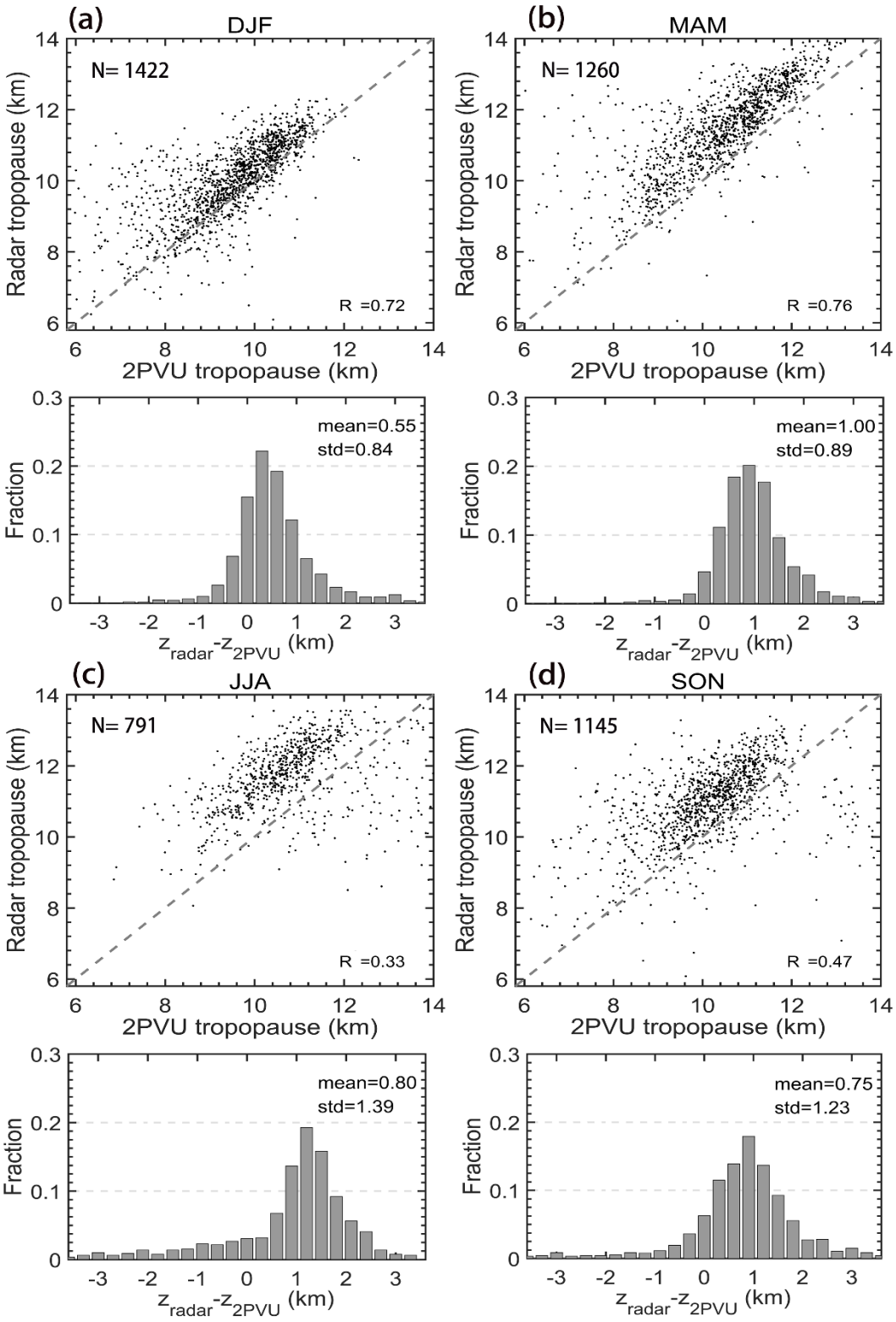

601

602 **Figure 6.** Same as figure 4, but for the comparison between the RT and the PVT.

603

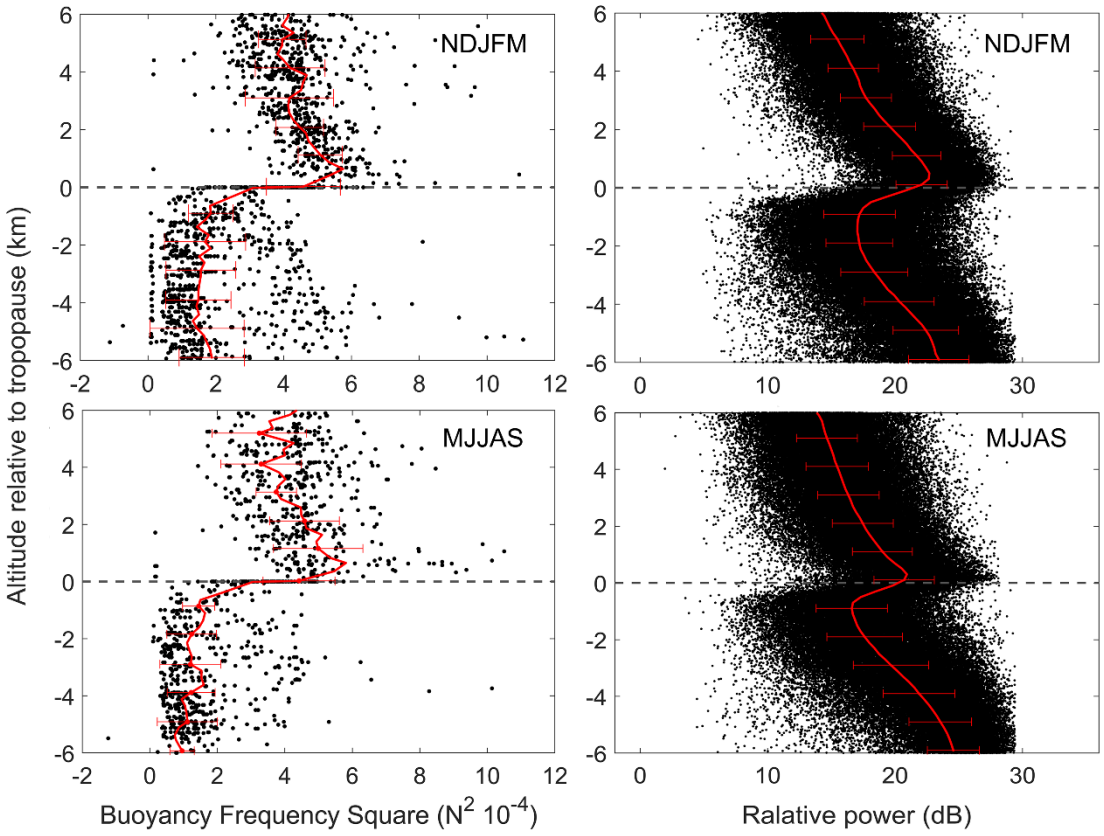

604

605 **Figure 7.** Scatterplots of (left panels) static stability (N^2) and (right panels) radar

606 relative echo power as a function of altitude relative to the LRT (left panels) and RT

607 (right panels) for extended winter (NDJFM) and summer (MJJAS) seasons for two

608 specific years 2012-2013. Red lines in each panel denote the corresponding mean

609 profiles and the error bars indicate the standard deviations.

610

611

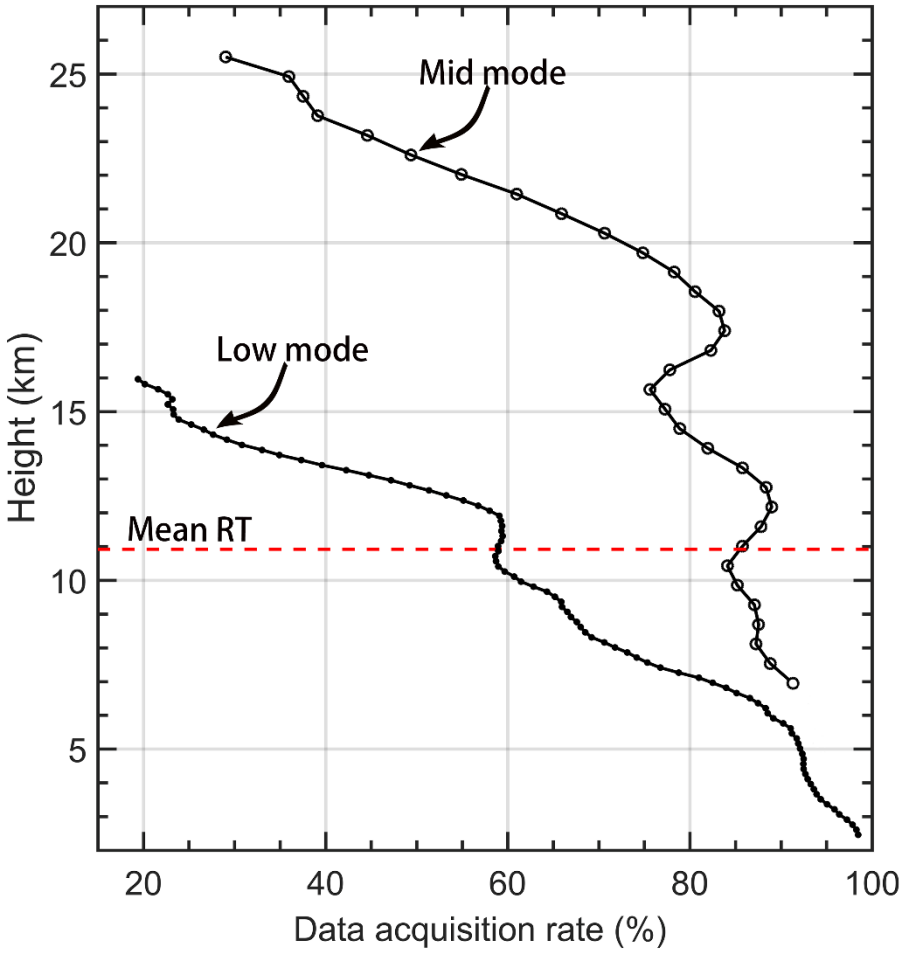

612

613 **Figure 8.** Vertical height profiles of the averaged effective radar wind data acquisition

614 rate in low mode and middle mode during November 2011-May 2017. The red dashed

615 line indicates the mean RT height.

616

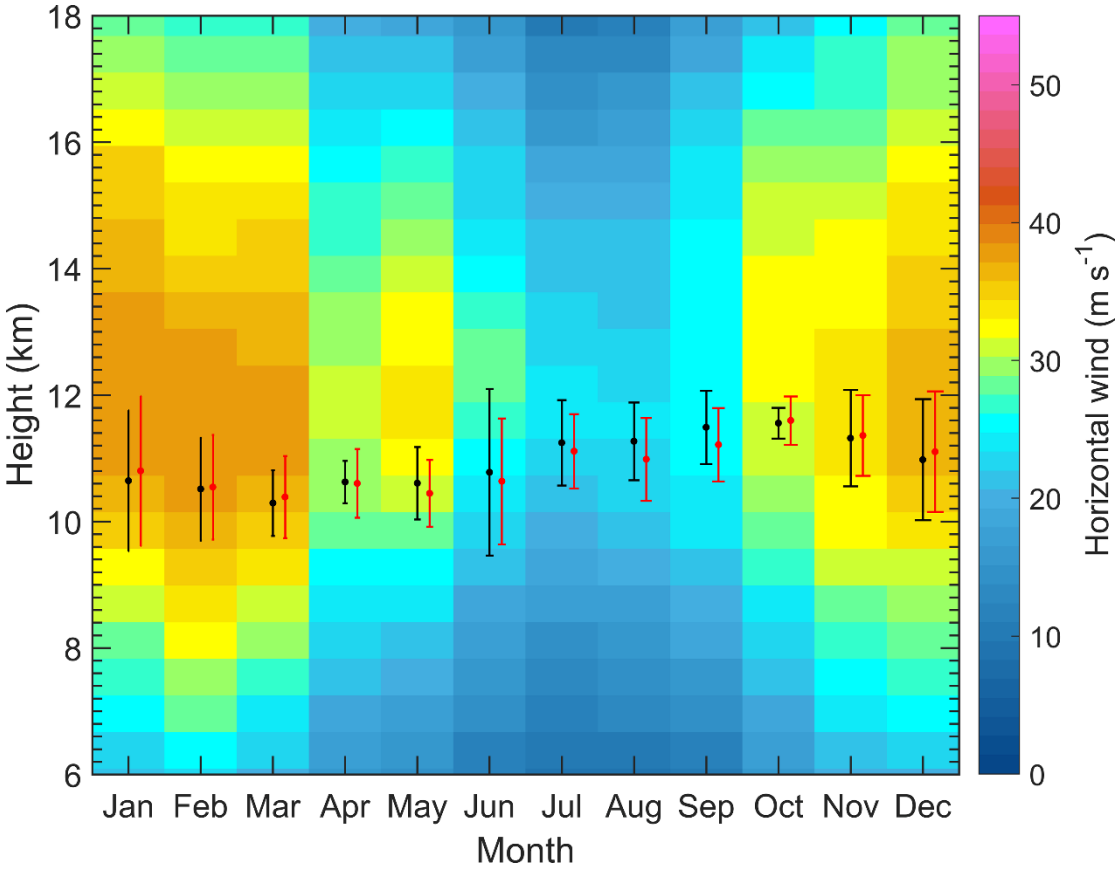

617

618 **Figure 9.** Height-time intensity map of monthly mean horizontal wind speed (shaded,

619 m/s) derived from the middle mode of Beijing MST radar, during November 2011-May

620 2017. Also shown is the monthly mean height of RT (black dots) and LRT (red dots,

621 offset by +6 days) along with the vertical error bars representing the standard deviations.

622

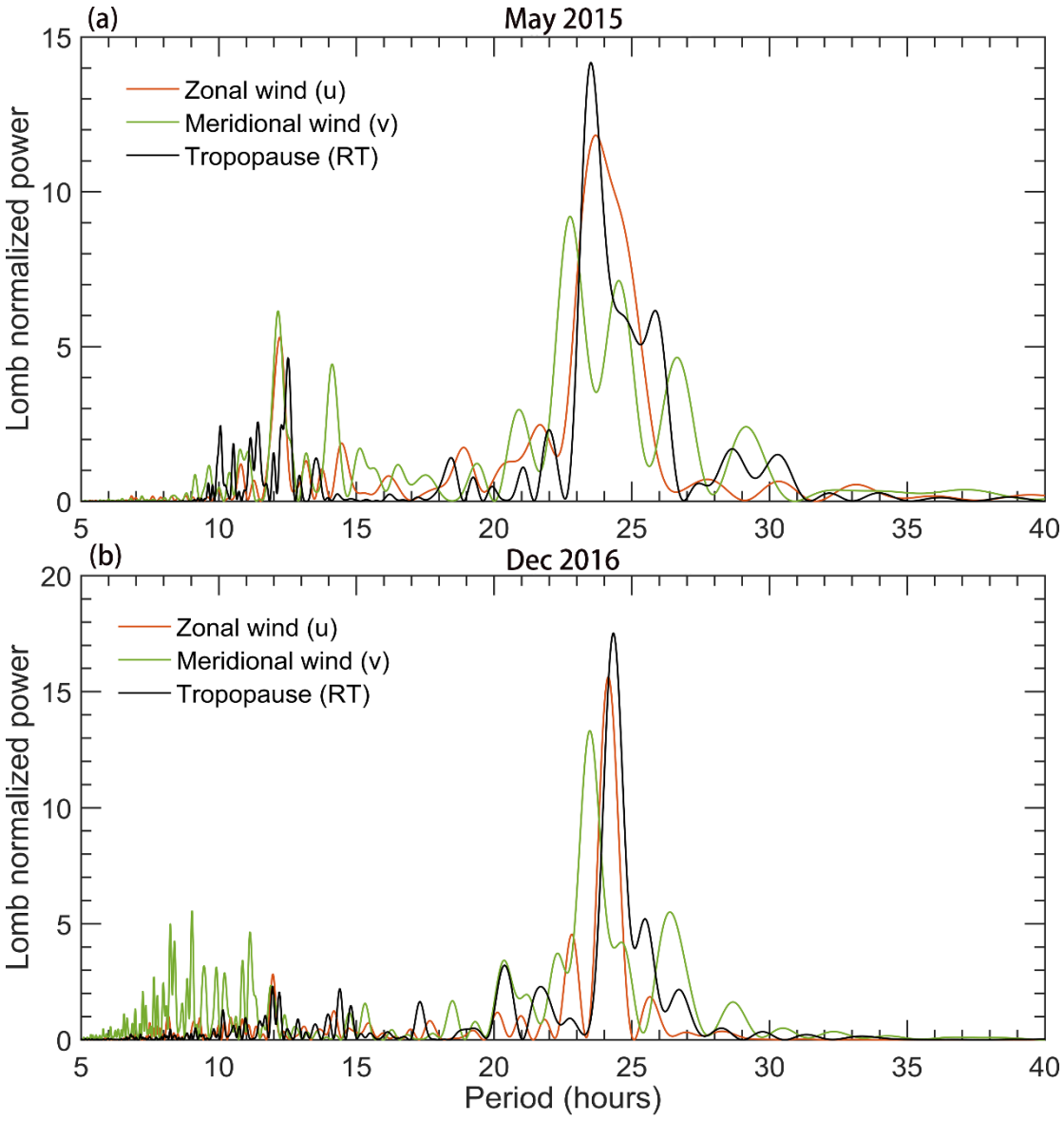

623

624 **Figure 10.** Lomb-Scargle periodograms of the RT height, zonal, and meridional wind

625 oscillations for specific months of (a) May 2015 and (b) December 2016. The zonal and

626 meridional wind for (a) is sampled at 9.85 km and (b) at 11 km.

627

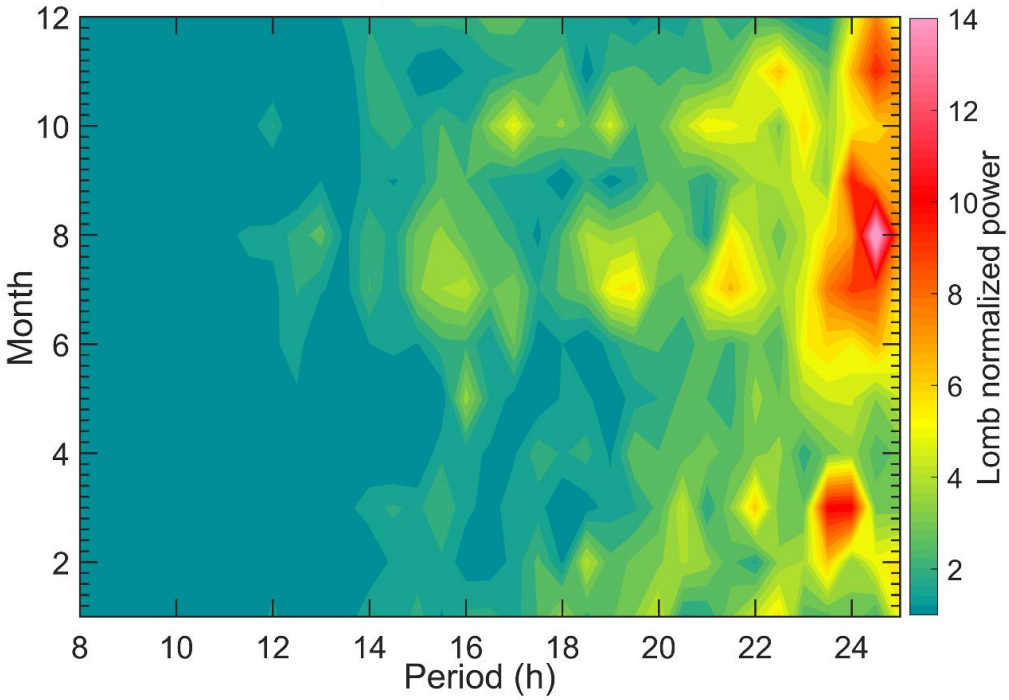

628

629 **Figure 11.** Mean Lomb-Scargle periodograms of RT height as a function of the time of

630 month during November 2011-May 2017.

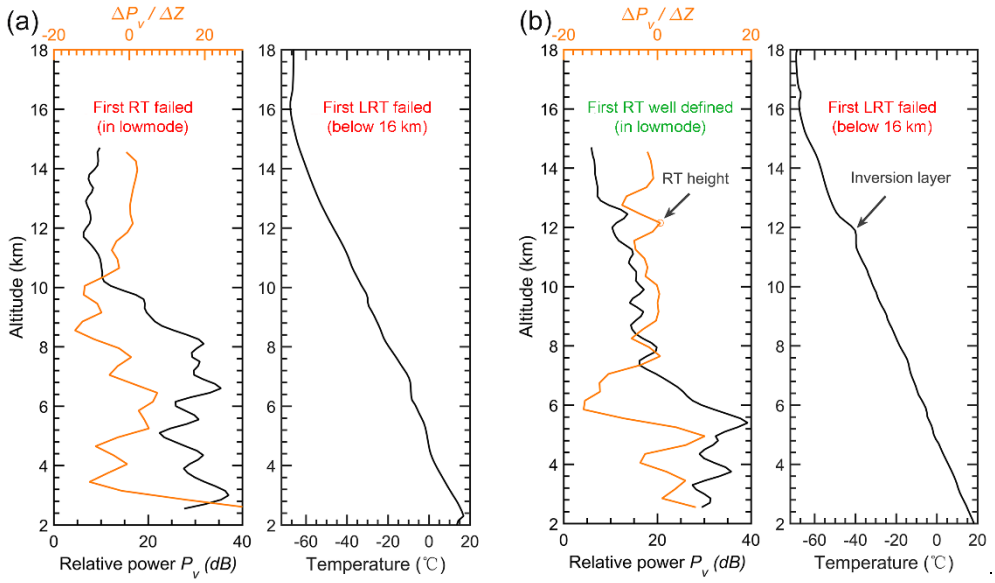

631

632 **Figure 12.** Example profiles of radar echo power and radiosonde temperature that (a)

633 both the RT and LRT definitions fail due to the continuing decrease in temperature on

634 00 UTC 7 July 2012 and (b) the temperature inversion layer failed to meet the LRT

635 definition but well defined in RT definition on 12 UTC 02 August 2012. Please note

636 that we only consider the conditions below 16 km.